Convergence Constrained Multiuser Transmitter-Receiver Optimization in Single Carrier FDMA

Valtteri Tervo*, *Student Member, IEEE,* Antti Tölli, *Member, IEEE,* Juha Karjalainen, *Member, IEEE,* Tad Matsumoto, *Fellow, IEEE*

***Abstract*—Convergence constrained power allocation (CCPA) in single carrier multiuser (MU) single-input multiple-output (SIMO) systems with turbo equalization is considered in this paper. In order to exploit the full benefit of the iterative receiver, its convergence properties need to be taken into account also at the transmitter side. The proposed scheme can guarantee that the desired quality of service (QoS) is achieved after a sufficient number of iterations. We propose two different successive convex approximations for solving the non-convex power minimization problem subject to user specific QoS constraints. The results of an extrinsic information transfer (EXIT) chart analysis demonstrate that the proposed CCPA scheme can achieve the design objective. Numerical results show that the proposed schemes can achieve superior performance in terms of power consumption as compared to linear receivers with and without precoding, as well as to the iterative receiver without precoding.**

***Index Terms*—Power minimization, soft interference cancellation, MMSE receiver, multiuser detection**

I. Introduction

Frequency domain equalization (FDE) for single-carrier transmission [1] and multi-carrier schemes based on orthogonal division multiplexing (OFDM) [2] are known as efficient techniques for tackling the inter-symbol-interference (ISI) problem in frequency selective fading channels. Both of the aforementioned techniques can be extended to multiuser communications yielding single-carrier frequency division multiple access (FDMA) [3] and orthogonal frequency division multiple access (OFDMA) [4], respectively. In OFDMA all available subcarriers are grouped into different subchannels[1] that are assigned to distinct users. User separation at the receiver side is straightforward due to the orthogonality of the subchannels.

Single-carrier FDMA can be viewed as a form of OFDMA in which an extra discrete fourier transform (DFT) and an inverse DFT (IDFT) are added at the transmitter and receiver sides, respectively. The DFT precoder spreads all the symbols across the whole frequency band forming a virtual single carrier structure. The advantage of FDMA compared to OFDMA is its lower peak-to-average power ratio (PAPR). However, optimal multi-user detection in single carrier FDMA in the presence of a frequency selective channel results in a prohibitively high computational complexity. A linear minimum mean squared error (LMMSE) detector provides an attractive low complexity scheme for the detection of an FDMA signal in the presence of ISI and multiuser interference (MUI) utilizing the circulant structure of channel matrices [5], [6].

An iterative FDE technique can achieve a significant performance gain over linear FDE in ISI channels [6]. In iterative FDE, the key idea is to utilize the feedback from a soft-output forward error correction (FEC) decoder that is updated according to "turbo" principle. To exploit the full merit of an iterative receiver, the convergence properties of a receiver based on the "turbo" principle needs to be taken into account jointly at the transmitter and the receiver. In [7], an extrinsic information transfer (EXIT) analysis [8] is utilized to determine optimal power allocation in a multiuser turbo coded code division multiple access (CDMA) system. In [9], a convergence analysis for MMSE based iterative equalizer is performed by using signal-to-noise power ratio (SNR) variance charts [6]. Furthermore, the authors in [9] use the convergence analysis to formulate a transmitter power allocation problem in frequency selective single-input single-output (SISO) channels with the iterative receiver mentioned above, assuming the availability of perfect channel state information (CSI) both at the transmitter and the receiver. In [10], [11], the impact of precoder design on convergence properties of the soft cancellation (SC) frequency domain (FD) minimum mean-squared error (MMSE) equalizer is demonstrated. In [12], a precoder design for multiuser (MU) multiple-input multiple-output (MIMO) ISI channels based on iterative LMMSE detection is considered. The design criterion of the precoder in [12] is to maximize the signal-to-interference and noise ratio (SINR) at the end of the iterative process. In [13], an in-depth analysis of the power allocation problem in single-carrier MIMO systems with iterative FD-SC-MMSE equalization has been presented.

This work was supported by the Finnish Funding Agency for Technology and Innovation (TEKES), the Academy of Finland, Riitta and Jorma J. Takanen Foundation, the Finnish Foundation for Technology Promotion, Walter Ahlström Foundation, Ulla Tuominen foundation and KAUTE-foundation. This work was also in part supported by the Japanese government funding program, Grant-in-Aid for Scientific Research (B), No. 23360170. A part of the material in this paper was presented at the Annual Conference on Signals, Systems, and Computers, Pacific Grove, CA, USA, November 4-7, 2012.

V. Tervo and T. Matsumoto are with the Centre for Wireless Communications, University of Oulu, P.O. Box 4500, 90014 University of Oulu, Finland, and Japan Advanced Institute of Science and Technology, 1-1 Asahi-Dai, Nomi, Ishikawa, 923-1292 Japan, email: {wade, matumoto}@ee.oulu.fi.

A. Tölli is with the Centre for Wireless Communications, University of Oulu, email: atolli@ee.oulu.fi.

J. Karjalainen is with the Nokia Networks, Kaapelitie 4, 90620, Oulu, Finland, email: juha.p1.karjalainen@nokia.com.

[1]The bandwidth of each subchannel is less than the coherence bandwidth of the channel which results in flat fading subchannels.

The EXIT chart is one of the most powerful tools for analyzing and optimizing parameters in iterative processing [14]–[16]. The convergence of an iterative process can be predicted by investigating the exchange of extrinsic information of the soft in / soft out (SftI/SftO) blocks in the form of mutual information (MI) between transmitted bits and the corresponding log-likelihood ratios (LLRs). The analysis can be made independently for each block, which eliminates the necessity of time consuming chain simulations. When applied to a joint equalizer and FEC decoder design, the objective is to guarantee an open convergence tunnel between the equalizer's and the decoder's EXIT functions. To be more specific, the EXIT function of the equalizer has to be above the inverse EXIT function of the decoder until so called MI convergence point, which determines the communication reliability represented by bit error probability (BEP) achieved by the iterative equalizer. Therefore, the width of the tunnel as well as the MI convergence point are the key parameters when optimizing an iterative process using the EXIT charts [17], [18].

The contributions of this paper are summarized as follows: we extend the convergence constrained power minimization problem [13] to the multiuser (MU) single-input multiple-output (SIMO) system which results in a joint optimization of multiple transmitters and the iterative receiver. The presence of multiple users leads to multidimensional EXIT functions, which makes the optimization very complex as such. We present a suboptimal solution referred to as *diagonal sampling* in Section IV-B. In [13], only quadrature phase sift keying (QPSK) modulation is considered. In this paper, we also derive a heuristic approach for 16-ary quadrature amplitude modulation (16QAM). The aim is to minimize the power consumption in single-carrier FDMA with iterative detection subject to a quality of service (QoS) constraint. This can be adopted for example in long term evolution (LTE) type of systems [19]. Unlike in [13] the joint optimization of the multiple transmitters and the receiver is not convex. Thus, we use a block coordinate descent (BCD) method [20] where the non-convex joint optimization problem is split to separate transmitter and receiver optimization problems. Furthermore, we show that the MMSE receiver is a power minimizing receiver and therefore, the objective value in the alternating optimization converges to a local solution. However, unlike the power minimization problem with the classical per subcarrier SINR constraint [21], the problem considered in this paper cannot be formulated as a convex even for a fixed receiver. Therefore, two efficient algorithms based on a successive convex approximation (SCA) method [22] are proposed for solving the transmitter optimization problem for fixed receive beamformers.

The rest of the paper is organized as follows: A system model of a single carrier uplink transmission with multiple single-antenna users and a base station with multiple antennas is presented in Section II. In Section III, an iterative frequency domain equalizer is described. Convergence constrained power allocation (CCPA) for turbo equalizer is derived in Section IV. In Section V, algorithms for solving the CCPA problem are derived. Performance of proposed algorithms is demonstrated through simulations in Section VI. Finally, conclusions are drawn in Section VII.

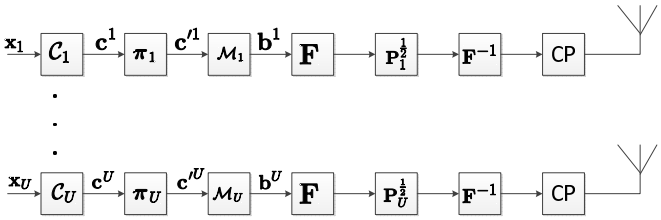

Fig. 1. The block diagram of the transmitter side of the system model.

Nomenclature **–** The following notations are used throughout the paper: Vectors are denoted by lower boldface letters and matrices by uppercase boldface letters. The superscripts $^{\mathrm{H}}$ and $^{\mathrm{T}}$ denote Hermitian and transposition of a complex vector or matrix, respectively. $\mathbb{C}$, $\mathbb{R}$, $\mathbb{B}$ denote complex, real and binary number fields, respectively. $\mathbf{I}_N$ denotes $N \times N$ identity matrix. The operator $\mathrm{avg}\{\cdot\}$ calculates the arithmetic mean of its argument, $\mathrm{diag}(\cdot)$ generates diagonal matrix of its arguments, $\mathrm{bdiag}\{\cdot\}$ generates the block diagonal matrix from its argument matrices, $\otimes$ denotes the Kronecker product and $||\cdot||$ is the Euclidean norm of its complex argument vector.

II. System Model

Consider uplink transmission with U single antenna users and a base station with N_R antennas. The transmitter side of the system model is depicted in Fig. 1. Each user's data stream $\mathbf{x}_u \in \mathbb{B}^{R_c^u N_Q N_F}$, $u = 1, 2, \ldots, U$, is encoded by FEC code $\mathcal{C}_u$ with a code rate $R_c^u \leq 1$. N_Q denotes the number of bits per modulation symbol and N_F is the number of frequency bins in discrete Fourier transform (DFT). Encoded bits $\mathbf{c}^u = [c_1^u, c_2^u, \ldots, c_{N_Q N_F}]^{\mathrm{T}} \in \mathbb{B}^{N_Q N_F}$ are bit-interleaved by multiplying $\mathbf{c}^u$ by pseudo-random permutation matrix $\boldsymbol{\pi}_u \in \mathbb{B}^{N_Q N_F \times N_Q N_F}$ resulting in a bit sequence $\mathbf{c}'^u = \boldsymbol{\pi}_u \mathbf{c}^u$. After the interleaving, the sequence $\mathbf{c}'^u$ is mapped with a mapping function $\mathcal{M}_u(\cdot)$ onto a 2^{N_Q}-ary complex symbol $b_l^u \in \mathbb{C}$, $l = 1, 2, \ldots, N_F$, resulting in a complex data vector $\mathbf{b}^u = [b_1^u, b_2^u, \ldots, b_{N_F}^u]^{\mathrm{T}} \in \mathbb{C}^{N_F}$. Each user's modulated data stream is spread across the subchannels by multiplying $\mathbf{b}^u$ by a DFT matrix $\mathbf{F} \in \mathbb{C}^{N_F \times N_F}$, $\forall u = 1, 2, \ldots, U$,[2]. The elements of $\mathbf{F}$ are given by

$$f_{m,l} = \frac{1}{\sqrt{N_F}} e^{(i2\pi(m-1)(l-1)/N_F)} \tag{1}$$

with $m, l = 1, 2, \ldots, N_F$. Each user's data stream is multiplied with its associated power allocation matrix $\mathbf{P}_u^{\frac{1}{2}}$, where $\mathbf{P}_u = \mathrm{diag}([P_{u,1}, P_{u,2}, \ldots, P_{u,N_F}]^{\mathrm{T}}) \in \mathbb{R}^{N_F \times N_F}$, with $P_{u,l}$ being the power allocated to the lth frequency bin. Finally, before transmission, each user's data stream is transformed into the time domain by the inverse DFT (IDFT) matrix $\mathbf{F}^{-1}$ and a cyclic prefix is added to mitigate the inter-block interference (IBI).

The receiver side of the system model is depicted in Fig. 2. After the cyclic prefix removal, the signal can be expressed

[2]The same amount of frequency domain resources are assumed to be allocated for each user in a cell.

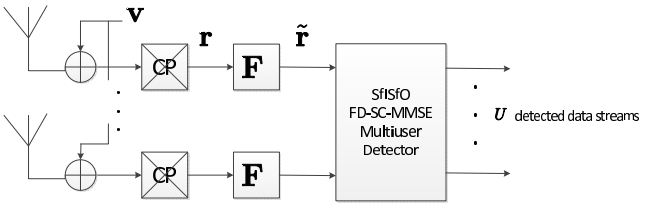

Fig. 2. The block diagram of the receiver side of the system model.

as[3]

$$\mathbf{r} = \mathbf{H}_u \mathbf{F}^{-1} \mathbf{P}_u^{\frac{1}{2}} \mathbf{F} \mathbf{b}^u + \sum_{y \neq u}^{U} \mathbf{H}_y \mathbf{F}^{-1} \mathbf{P}_y^{\frac{1}{2}} \mathbf{F} \mathbf{b}^y + \mathbf{v}, \quad (2)$$

where $\mathbf{H}_u = [\mathbf{H}_u^1, \mathbf{H}_u^2, \ldots, \mathbf{H}_u^{N_R}]^{\mathrm{T}} \in \mathbb{C}^{N_R N_F \times N_F}$ is the space-time channel matrix for user u and $\mathbf{H}_u^r = \mathrm{circ}\{[h_{u,1}^r, h_{u,2}^r, \ldots, h_{u,N_L}^r, \mathbf{0}_{1\times N_F - N_L}]^{\mathrm{T}}\} \in \mathbb{C}^{N_F \times N_F}$ is the time domain circulant channel matrix for user u at the receive antenna r. The operator circ$\{\}$ generates a matrix that has a circulant structure of its argument vector, N_L denotes the length of the channel impulse response, and $h_{u,l}^r$, $l = 1, 2, \ldots, N_L$, $r = 1, 2, \ldots, N_R$, is the fading factor of multipath channel. A vector $\mathbf{v} \in \mathbb{C}^{N_R N_F}$ in (2) denotes white additive independent identically distributed (i.i.d.) Gaussian noise vector with variance σ^2. The signal $\mathbf{r}$ is transformed into the frequency domain by using DFT matrix $\mathbf{F}_{N_R} = \mathbf{I}_{N_R} \otimes \mathbf{F} \in \mathbb{C}^{N_R N_F \times N_R N_F}$, resulting in

$$\tilde{\mathbf{r}} = \mathbf{\Gamma} \mathbf{P}^{\frac{1}{2}} \mathbf{F}_U \mathbf{b} + \mathbf{F}_{N_R} \mathbf{v}, \quad (3)$$

where $\mathbf{\Gamma} = [\mathbf{\Gamma}_1, \mathbf{\Gamma}_2, \ldots, \mathbf{\Gamma}_U] \in \mathbb{C}^{N_R N_F \times U N_F}$ with $\mathbf{\Gamma}_u = \mathrm{bdiag}\{\mathbf{\Gamma}_{u,1}, \mathbf{\Gamma}_{u,2}, \ldots, \mathbf{\Gamma}_{u,N_F}\} \in \mathbb{C}^{N_R N_F \times N_F}$ being the space-frequency channel matrix for user u expressed as

$$\mathbf{\Gamma}_u = \mathbf{F}_{N_R} \mathbf{H}_u \mathbf{F}^{-1}. \quad (4)$$

$\mathbf{\Gamma}_{u,m} \in \mathbb{C}^{N_R \times N_R}$ is the diagonal channel matrix for the m^{th} frequency bin of the u^{th} user, $\mathbf{F}_U = \mathbf{I}_U \otimes \mathbf{F} \in \mathbb{C}^{U N_F \times U N_F}$, and $\mathbf{b} = [\mathbf{b}^{1^{\mathrm{T}}}, \mathbf{b}^{2^{\mathrm{T}}}, \ldots, \mathbf{b}^{U^{\mathrm{T}}}]^{\mathrm{T}} \in \mathbb{C}^{U N_F}$. The power allocation matrix is composed by $\mathbf{P} = \mathrm{diag}(\mathbf{P}_1, \mathbf{P}_2, \ldots, \mathbf{P}_U) \in \mathbb{R}^{U N_F \times U N_F}$.

III. Receiver

The block diagram of the frequency domain turbo equalizer is depicted in Fig. 3. Frequency domain signal after the soft cancelation can be written as

$$\hat{\mathbf{r}} = \tilde{\mathbf{r}} - \mathbf{\Gamma} \mathbf{P}^{\frac{1}{2}} \mathbf{F}_U \tilde{\mathbf{b}}, \quad (5)$$

where $\tilde{\mathbf{b}} = [\tilde{\mathbf{b}^1}^{\mathrm{T}}, \tilde{\mathbf{b}^2}^{\mathrm{T}}, \ldots, \tilde{\mathbf{b}^U}^{\mathrm{T}}]^{\mathrm{T}} \in \mathbb{C}^{U N_F}$ is composed by $\tilde{\mathbf{b}}^u = [\tilde{b}_1^u, \tilde{b}_2^u, \ldots, \tilde{b}_{N_F}^u]^{\mathrm{T}} \in \mathbb{C}^{N_F}$. The soft symbol estimate $\tilde{b}_n^u$ is calculated as [13]

$$\tilde{b}_n^u = E\{b_n^u\} = \sum_{b_i \in \mathfrak{B}} b_i \Pr(b_n^u = b_i), \quad (6)$$

[3]In this paper, single cell scenario is considered and the impact of inter-cell-interference is excluded.

where $\mathfrak{B}$ is the modulation symbol alphabet, and the symbol *a priori* probability can be calculated by [23]

$$\begin{aligned} \Pr(b_n^u = b_i) &= \prod_{q=1}^{N_Q} \Pr({c'}^u_{N_Q(n-1)+q} = s_{i,q}) \\ &= \left(\frac{1}{2}\right)^{N_Q} \prod_{q=1}^{N_Q} (1 - \bar{s}_{i,q} \tanh(\mathring{L}'^u_{(n-1)N_Q+q}/2)), \end{aligned} \quad (7)$$

with $\bar{s}_{i,q} = 2 s_{i,q} - 1$ and $\mathbf{s}_i = [s_{i,1}, s_{i,2}, \ldots, s_{i,N_Q}]^{\mathrm{T}}$ is the binary representation of the symbol b_i, depending on the mapping rule for modulation. $\mathring{L}'^u_{(n-1)N_Q+q}$ is the *a priori* LLR of the bit ${c'}^u_{N_Q(n-1)+q}$, provided by the decoder of user u. After the soft cancelation, the residual and the estimated received signal of user u are summed up, yielding $\breve{\mathbf{r}}_u \in \mathbb{C}^{N_R N_F}$ as [24]

$$\breve{\mathbf{r}}_u = \hat{\mathbf{r}} + \mathbf{\Gamma}_u \mathbf{P}_u^{\frac{1}{2}} \mathbf{F} \tilde{\mathbf{b}}^u. \quad (8)$$

The time domain output of the receive filter for the u^{th} user can be written as

$$\hat{\mathbf{b}}^u = \mathbf{F}^{-1} \breve{\mathbf{\Omega}}_u^{\mathrm{H}} \breve{\mathbf{r}}_u, \quad (9)$$

where $\breve{\mathbf{\Omega}}_u = [\breve{\mathbf{\Omega}}_u^1, \breve{\mathbf{\Omega}}_u^2, \ldots, \breve{\mathbf{\Omega}}_u^{N_R}]^{\mathrm{T}} \in \mathbb{C}^{N_R N_F \times N_F}$ is the filtering matrix for the u^{th} user and $\breve{\mathbf{\Omega}}_u^r \in \mathbb{C}^{N_F \times N_F}$ is the filtering matrix for the r^{th} receive antenna of the u^{th} user. The effective SINR of the prior symbol estimates for the u^{th} user after FEC decoding can be expressed as

$$\zeta_u = \frac{1}{N_F} \sum_{m=1}^{N_F} \frac{P_{u,m} \boldsymbol{\omega}_{u,m}^{\mathrm{H}} \boldsymbol{\gamma}_{u,m} \boldsymbol{\gamma}_{u,m}^{\mathrm{H}} \boldsymbol{\omega}_{u,m}}{\boldsymbol{\omega}_{u,m}^{\mathrm{H}} \mathbf{\Sigma}_{\hat{\mathbf{r}},m} \boldsymbol{\omega}_{u,m}}, \quad (10)$$

where $\boldsymbol{\gamma}_{u,m} \in \mathbb{C}^{N_R}$ consists of the diagonal elements of $\mathbf{\Gamma}_{u,m}$, i.e., $\boldsymbol{\gamma}_{u,m}$ is the channel vector for the m^{th} frequency bin of user u. $\boldsymbol{\omega}_{u,m} = \left[[\breve{\mathbf{\Omega}}_u^1]_{[m,m]}, [\breve{\mathbf{\Omega}}_u^2]_{[m,m]} \ldots, [\breve{\mathbf{\Omega}}_u^{N_R}]_{[m,m]}\right]^{\mathrm{T}} \in \mathbb{C}^{N_R}$ is the receive beamforming vector for the m^{th} frequency bin of user u, and $\mathbf{\Sigma}_{\hat{\mathbf{r}},m} \in \mathbb{C}^{N_R \times N_R}$ is the interference covariance matrix of the m^{th} frequency bin given by

$$\mathbf{\Sigma}_{\hat{\mathbf{r}},m} = \sum_{l=1}^{U} P_{l,m} \boldsymbol{\gamma}_{l,m} \boldsymbol{\gamma}_{l,m}^{\mathrm{H}} \bar{\Delta}^l + \sigma^2 \mathbf{I}_{N_R}. \quad (11)$$

$\bar{\Delta}^l = \mathrm{avg}\{\mathbf{1}_{N_F} - \ddot{\mathbf{b}}^l\}$ is the average residual interference of the soft symbol estimates and $\ddot{\mathbf{b}}^l = [|\tilde{b}_1^l|^2, |\tilde{b}_2^l|^2, \ldots, |\tilde{b}_{N_F}^l|^2]^{\mathrm{T}} \in \mathbb{C}^{N_F}$. The scalar $\bar{\Delta}^l = \mathrm{avg}\{\mathbf{1}_{N_F} - \ddot{\mathbf{b}}^l\}$ is an approximation which is reasonably accurate for normalized 2^{N_Q}-ary PSK as well as for rectangular 2^{N_Q}-ary QAM with an appropriate normalization [13]. For QAM, both the transmitted symbol vector $\mathbf{b}^u$ and soft-symbol vector $\tilde{\mathbf{b}}^u$ have to be multiplied by the normalization factor $\kappa = \sqrt{\frac{3}{2(2^{N_Q}-1)}}$.

IV. Convergence Constrained Power Allocation

In this section, the joint power allocation and receive beamforming optimization problem for the iterative receiver is formulated. The general problem formulation follows from [13] where CCPA is derived for single user MIMO systems. However, the major difference compared to [13] is that the EXIT space now has $U + 1$ dimensions.

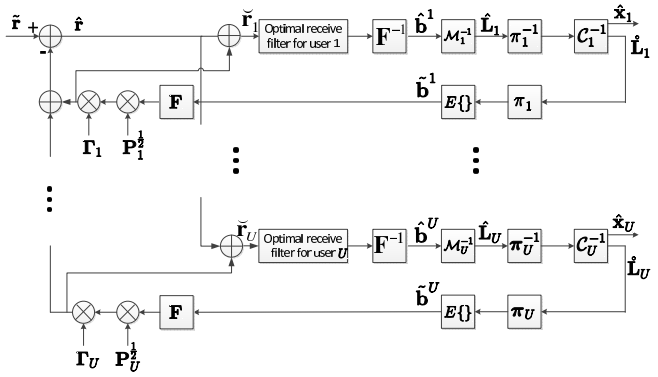

Fig. 3. The block diagram of frequency domain turbo equalizer.

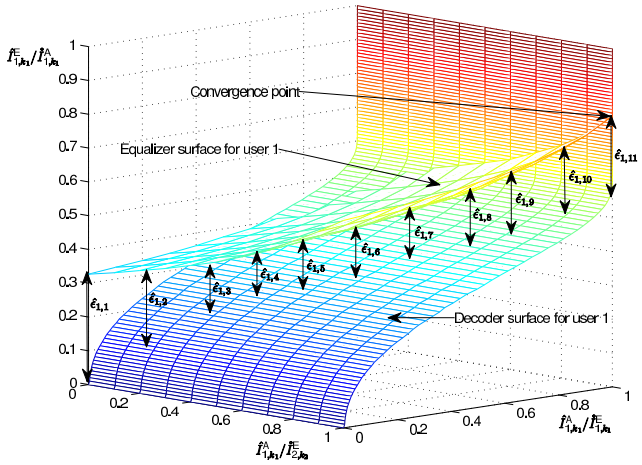

Fig. 4. An example of 3 dimensional formulation of the problem for user 1. $U = 2$, $N_F = 8$, $N_R = 1$, $K = 11$, $\hat{I}_u^{\mathrm{E,target}} = 0.8$, $\mathring{I}_u^{\mathrm{E,target}} = 0.9999$, $\epsilon_u = 0.1$, $u = 1, 2$, $R_c = 1/3$, $N_L = 5$.

This section is outlined as follows: first of all, the general problem formulation for multiuser SIMO systems is provided. We demonstrate that the convergence is guaranteed as long as there exists an open tunnel between the $U+1$-dimensional EXIT surfaces until the desired MI point. After that, we introduce a novel *diagonal sampling* approach which makes the problem solvable without performing exhaustive search. We also show how to transfer the MI constraints to LLR variance constraints in the case of BPSK and QPSK. Finally, we apply CCPA to the case of 16QAM and show that the proposed convergence constraint guarantees the convergence for 16QAM as well. Gray mapping is assumed as a modulation mapping throughout the derivation.

A. General Problem Formulation

Let $\hat{I}_u^{\mathrm{E}}$ denote the average MI between the transmitted interleaved coded bits $\mathbf{c}'^u$ and the LLRs $\hat{\mathbf{L}}_u$ at the output of the equalizer [13, Eq. (18)]. For notational convenience, equalizer refers to the combined block of the receive filter and soft mapper / demapper. Similarly to [13] maximum a posteriori (MAP) soft demapper / mapper is used in this paper. Moreover, let $\hat{I}_u^{\mathrm{A}}$ denote the *a priori* MI at the input of the equalizer and $\hat{f}_u : [0,1]^U \rightarrow [0,1]$ denote a monotonically increasing EXIT function of the equalizer of the u^{th} user. Similarly, let $\mathring{I}_u^{\mathrm{E}}$ denote the average MI between the transmitted coded bits $\mathbf{c}^u$ and the LLRs $\mathring{\mathbf{L}}_u$ at the output of the decoder and $\mathring{f}_u : [0,1] \rightarrow [0,1]$ denote a monotonically increasing EXIT function of the decoder of the u^{th} user. The essential condition for the convergence of the turbo equalizer can be written as

$$\exists\{\mathring{I}_i^{\mathrm{E}} \in [0,1]\}_{\substack{i=1 \\ i\neq u}}^{U} : \hat{f}_u(\mathring{I}_1^{\mathrm{E}}, \ldots, \mathring{I}_u^{\mathrm{E}}, \ldots, \mathring{I}_U^{\mathrm{E}}) \geq \mathring{f}_u^{-1}(\mathring{I}_u^{\mathrm{E}}) + \epsilon_u(\mathring{I}_u^{E}), \forall u = 1, 2 \ldots, U, \quad (12)$$

i.e., for all u, there exists a set of outputs from the decoders of all the users except u such that the EXIT function of the equalizer of user u is above the inverse of the EXIT function of the decoder of user u plus $\epsilon_u(\mathring{I}_u^{E})$ which is a function controlling the minimum gap between the $U+1$-dimensional EXIT function of the equalizer of user u and the inverse of the decoder's EXIT function of user u. In other words, the convergence is guaranteed as long as there exists an open tunnel between the two EXIT surfaces until the convergence point. The constraint (12) is much more challenging to deal with than [13] where the EXIT chart is 2-dimensional. This is illustrated in the case of two users in Fig. 4 where we can see the impact of the *a priori* information input from the other user's decoder.

We demonstrate that (12) guarantees the convergence: Let $U = 2$ and assume that there exists an open tunnel between the EXIT surfaces until the convergence point as presented in Fig. 4. Let $\mathring{I}_u^{\mathrm{E,target}}$, $0 \leq \mathring{I}_u^{\mathrm{E,target}} \leq 1$, be the target MI point of user u after iterations. Furthermore, let $i_u \in \mathbb{N}$ be the index of iteration and $\mathring{I}_{u,i_u}^{\mathrm{E}}$ denote the MI after iteration i_u such that $\mathring{I}_{u,i_u+1}^{\mathrm{E}} \geq \mathring{I}_{u,i_u}^{\mathrm{E}}$. Focusing on the user 1, the condition (12) is written

$$\hat{f}_1(\mathring{I}_1^{\mathrm{E}}, \mathring{I}_2^{\mathrm{E}}) \geq \mathring{f}_1^{-1}(\mathring{I}_1^{\mathrm{E}}) + \epsilon_1(\mathring{I}_1^{E}), \quad (13)$$

such that for each $\mathring{I}_{1,i_1}^{\mathrm{E}}$, $0 \leq \mathring{I}_{1,i_1}^{\mathrm{E}} \leq \mathring{I}_1^{\mathrm{E,target}}$, there exists at least one $\mathring{I}_{2,i_2}^{\mathrm{E}}$, $0 \leq \mathring{I}_{2,i_2}^{\mathrm{E}} \leq \mathring{I}_2^{\mathrm{E,target}}$ that satisfies the condition. Let the output value after the first activation of the decoder 1 be $\mathring{I}_{1,1}^{\mathrm{E}}$, such that (13) holds for some $\mathring{I}_{2,\tilde{i}_2}^{\mathrm{E}}$. Due to the monotonicity of the EXIT function the condition (13) holds for all indices $i_2 \geq \tilde{i}_2$. Activating the decoder of user 1 again, the output of the equalizer is then given by $\hat{f}_1(\mathring{I}_{1,2}^{\mathrm{E}}, \mathring{I}_{2,\tilde{i}_2}^{\mathrm{E}})$. If the condition (13) does not hold at the point $(\mathring{I}_1^{\mathrm{E}}, \mathring{I}_2^{\mathrm{E}}, \mathring{I}_1^{\mathrm{E}}) = (\mathring{I}_{1,2}^{\mathrm{E}}, \mathring{I}_{2,\tilde{i}_2}^{\mathrm{E}}, \hat{f}_1(\mathring{I}_{1,2}^{\mathrm{E}}, \mathring{I}_{2,\tilde{i}_2}^{\mathrm{E}}))$ in the 3-dimensional EXIT chart, i.e., $\hat{f}_1(\mathring{I}_{1,2}^{\mathrm{E}}, \mathring{I}_{2,\tilde{i}_2}^{\mathrm{E}})) < \mathring{f}_1^{-1}(\mathring{I}_{1,2}^{\mathrm{E}}) + \epsilon_1(\mathring{I}_1^{E})$, there exists at least one $\mathring{I}_{2,i_2}^{\mathrm{E}}$ that satisfies (13). Hence, $\tilde{i}_2$ can be increased, i.e., decoder 2 can be activated until the condition holds[4]. This process can be repeated until the convergence point is reached.

To make the problem tractable, continuous convergence

[4]If $U > 2$, all the decoders (excluding the decoder of user 1) can be activated until (13) holds.

condition (12) is discretized and replaced with

$$\exists\Big\{\mathring{I}^{\mathrm{E}}_{i,k_i} \in [0,1] : k_i \in \{1,2,\ldots,K_i\}\Big\}_{\substack{i=1\\ i\neq u}}^{U} :$$
$$\hat{f}_u(\mathring{I}^{\mathrm{E}}_{1,k_1},\ldots,\mathring{I}^{\mathrm{E}}_{u,k_u},\ldots,\mathring{I}^{\mathrm{E}}_{U,k_U}) \geq \mathring{f}_u^{-1}(\mathring{I}^{\mathrm{E}}_{u,k_u}) + \epsilon_{u,k_u},$$
$$\forall k_u = 1,2,\ldots,K_u, \forall u = 1,2\ldots,U. \quad (14)$$

Note that the indices k_u, $u = 1,2,\ldots,U$ in (14) denote the points in the EXIT chart and not the indices of iterations in real chain simulations. We will use this definition in the remaining part of the paper.

B. Diagonal Sampling

In this section, we restrict our discussion to the minimum power problem only, i.e., the objective is to minimize the sum power with a constraint (14).

To ease the handling of the problem, let $K_u = K$, $\forall u = 1,2,\ldots,U$, i.e., the number of discrete points in the EXIT chart is the same for all users. Furthermore, let $\epsilon_{u,k_u} = \epsilon_u$, $\forall k_u < K$ and $\epsilon_{u,K} = 0$. Moreover, we assume that $\mathring{I}^{\mathrm{E}}_{u,k_u+1} > \mathring{I}^{\mathrm{E}}_{u,k_u}$, $\forall k_u = 1,2,\ldots,K-1$, i.e., the indexing is ordered such that the MI increases with the index.

A 3-dimensional EXIT chart for user 1 is depicted in Fig. 4 for the case of $U = 2$. $\hat{I}^{\mathrm{A}}_{1,k_1}/\mathring{I}^{\mathrm{E}}_{u,k_u}$, $u = 1,2$, denotes the *a priori* information for the equalizer of the user 1 provided by the decoder of user u. Double arrows with $\hat{\epsilon}_{1,k_1}$, $k_1 = 1,2,\ldots,11$, denote the actual gap that is obtained from simulations with a constraint (14) and are placed at the diagonal sample points where the condition (14) is checked. Since ϵ_{1,k_1} denotes the minimum gap between the EXIT surfaces it holds that $\hat{\epsilon}_{1,k_1} \geq \epsilon_{1,k_1}$. In this example, we have selected $K = 11$ even though in many cases smaller K is enough to guarantee the convergence. Intuitively, a sufficient value of K depends on the shape of the decoder EXIT function. However, this is left as a future study.

The number of constraints in (14) is KU. However, to find the minimum power solution with the constraint (14), we need to know how to select the optimal set of sample points from $\{\mathring{I}^{\mathrm{E}}_i \in [0,1]\}_{\substack{i=1\\ i\neq u}}^{U}$ for each $u = 1,2,\ldots,U$. For finding the best set of sample points, i.e., the path from origin to the convergence point which leads to a minimum power consumption, one should be able to check all the possible paths in $U+1$ dimensional EXIT space from origin to the convergence point and choose the one which gives the best result. This leads to a combinatorial optimization problem which is difficult to solve.

If the EXIT surfaces of the decoder and the equalizer do not intersect at any sampled point, the only active constraints are the ones where there is no *a priori* information available from the other users. This can be justified by assuming that the EXIT function is monotonically increasing with its arguments, i.e., $\hat{f}_u(\mathring{I}^{\mathrm{E}}_{1,k_1},\ldots,\mathring{I}^{\mathrm{E}}_{u,k_u},\ldots,\mathring{I}^{\mathrm{E}}_{U,k_U}) \leq \hat{f}_u(\mathring{I}^{\mathrm{E}}_{1,\tilde{k}_1},\ldots,\mathring{I}^{\mathrm{E}}_{u,\tilde{k}_u},\ldots,\mathring{I}^{\mathrm{E}}_{U,\tilde{k}_U})$ if $\mathring{I}^{\mathrm{E}}_{u,k_u} \leq \mathring{I}^{\mathrm{E}}_{u,\tilde{k}_u}$ $\forall u = 1,2,\ldots,U$. In such a case, we can write the constraint (14) as

$$\hat{f}_u(0,0,\ldots,0,\mathring{I}^{\mathrm{E}}_{u,k_u},0,\ldots,0) \geq \mathring{f}_u^{-1}(\mathring{I}^{\mathrm{E}}_{u,k_u}) + \epsilon_{u,k_u},$$
$$\forall u = 1,2\ldots,U, \forall k_u = 1,2,\ldots,K. \quad (15)$$

This is the tightest possible constraint and it clearly cannot provide the best solution because with high probability there is another sampling which guarantees the convergence with lower power consumption. However, if the user does not know the modulation coding scheme (MCS), i.e., FEC codes and mapping rules for modulation of other users at the transmitter, one may consider using the constraint (15) to guarantee the reliable communication.

A pragmatic approach is to check only the points in the $U+1$-dimensional EXIT space where all the decoder's outputs are equal, i.e., we check the K points on the line from the origin to the convergence point. In other words, $\bar{\Delta}^l$ in (11) is equal to $\bar{\Delta}_k$, $\forall l = 1,2,\ldots,U$, where $\bar{\Delta}_k$ is the average residual interference at the k^{th} MI index. Thus, we can replace the $U+1$-dimensional EXIT function of the equalizer by 2-dimensional function $\hat{f}_u(\mathring{I}^{\mathrm{E}}_{1,k},\ldots,\mathring{I}^{\mathrm{E}}_{u,k},\ldots,\mathring{I}^{\mathrm{E}}_{U,k}) := \hat{f}^{\mathrm{2D}}_u(\mathring{I}^{\mathrm{E}}_k)$ and the constraint is written as

$$\hat{f}^{\mathrm{2D}}_u(\mathring{I}^{\mathrm{E}}_k) \geq \mathring{f}_u^{-1}(\mathring{I}^{\mathrm{E}}_k) + \epsilon_{u,k}, \forall k = 1,2,\ldots,K, \forall u = 1,2\ldots,U. \quad (16)$$

This approximation technique is referred to as *diagonal sampling*, which is assumed throughout the remaining part of the paper.

C. BPSK / QPSK

Similarly to [13], the MI constraint of (14) can be transformed to variance constraint using the approximation of the inverse of the so called J-function [16]

$$\sigma_Z^2 = J^{-1}(I_Z) \approx \left(-\frac{1}{H_1}\log_2(1 - I_Z^{\frac{1}{H_3}}) \right)^{\frac{1}{H_2}}, \quad (17)$$

where σ_Z^2 is the LLR variance, I_Z is the MI, and the parameters H_1, H_2 and H_3 can be found by least squares (LS) curve fitting with the constellation constrained capacity (CCC) equation [25]. Now, the MI constraint of (16) can be written as

$$\hat{\sigma}^2_{u,k} \geq \mathring{\sigma}^2_{u,k},$$
$$\forall k = 1,2,\ldots,K, \forall u = 1,2\ldots,U, \quad (18)$$

where $\hat{\sigma}^2_{u,k} = \mathrm{J}^{-1}(\hat{f}^{\mathrm{2D}}_u(\mathring{I}^{\mathrm{E}}_k))$ is the variance of the conditional LLR distribution at the output of the equalizer of user u depending on the MI at the output of all the decoders and $\mathring{\sigma}^2_{u,k} = \mathrm{J}^{-1}(\mathring{f}_u^{-1}(\mathring{I}^{\mathrm{E}}_{u,k}) + \epsilon_{u,k})$ is the variance of the conditional LLR distribution at the input of the decoder of user u depending on the MI at the output of the decoder of user u.

In [13], a result presented in [26] is used to find an analytical expression of the LLR variance at the output of the equalizer in the case of QPSK. We can use the same result by noting that $\bar{\Delta}^l = \bar{\Delta}_k$ in (11) when diagonal sampling is used. The LLR variance at the output of the equalizer is calculated as [13, Eq. (17)]

$$\hat{\sigma}^2_{u,k} = \frac{4\zeta_{u,k}}{1 - \zeta_{u,k}\bar{\Delta}_k}. \quad (19)$$

Substituting (19) to (18) the convergence constraint is written as

$$\zeta_{u,k} \geq \xi_{u,k}, \forall u = 1,2\ldots,U, \forall k = 1,2,\ldots,K, \quad (20)$$

where

$$\xi_{u,k} = \frac{\mathring{\sigma}^2_{u,k}}{4 + \mathring{\sigma}^2_{u,k}\bar{\Delta}_k}, \tag{21}$$

is a constant that depends on the FEC code.

D. A Heuristic Approach for 16QAM

Similarly to QPSK case, the MI at the output of the demapper can be transformed to the variance of the conditional LLR distribution by using (17). However, the parameters H_1, H_2 and H_3 are found by fitting the function (17) with the corresponding 16QAM results [27]. Let J_2 and J_4 denote the J-functions for QPSK and 16QAM, respectively. With these notations, the MI constraint of (16) for 16QAM can be written as

$$\begin{aligned}\mathrm{J}_4^{-1}(\hat{f}_u^{\mathrm{2D}}(\mathring{I}_k^{\mathrm{E}})) \geq \mathrm{J}_4^{-1}(\mathring{f}_u^{-1}(\mathring{I}_{u,k}^{\mathrm{E}}) + \epsilon_{u,k}),\\ \forall k = 1, 2, \ldots, K, \forall u = 1, 2 \ldots, U.\end{aligned} \tag{22}$$

The difference in system models with different modulation schemes arises in the soft demapper. To achieve the final form of the convergence constraint in (20) we used the expression (19) where Gray mapped QPSK is assumed. With 16QAM, the mapping between the SINR and the variance of the LLR distributions used for the derivation of (20) does not hold anymore. However, substituting the parameter values from [27, Table I] to (17), it can be easily verified that $\mathrm{J}_4^{-1}(I_Z) \geq \mathrm{J}_2^{-1}(I_Z)$[5], $\forall I_Z \in [0, 1]$. Using this result, we can obtain that when modulation order increases, larger LLR variance is needed to achieve the same SINR, i.e.,

$$\mathrm{J}_4^{-1}(\hat{f}_u^{\mathrm{2D}}(\mathring{I}_k^{\mathrm{E}})) \geq \mathrm{J}_2^{-1}(\hat{f}_u^{\mathrm{2D}}(\mathring{I}_k^{\mathrm{E}})) = \frac{4\zeta_{u,k}}{1 - \zeta_{u,k}\bar{\Delta}_k}. \tag{23}$$

We can conclude that for 16QAM the convergence constraint (20) is conservative, i.e., the resulting EXIT curve of the equalizer is never above the true $\hat{I}_{u,k}^{\mathrm{E}}$, $\forall u, k$. Hence, the convergence constraint (20) guarantees the convergence even with 16QAM. It should be noticed that the difference in convergence constraint between the QPSK and 16QAM arises in (21) where $\mathring{\sigma}^2_{u,k}$ is obtained using either J_2^{-1} or J_4^{-1} depending on the modulation.

V. Transmitter - Receiver Optimization

In this section, algorithms for solving the transmitter-receiver (Tx-Rx) optimization problem is presented. In Section V-A, the joint Tx-Rx optimization problem is split into separate transmitter and receiver optimization problems, which is referred to as *alternating optimization*. The non-convex Tx optimization problem for a fixed Rx is considered in Sections V-B and V-C.

The power minimization problem with the convergence constraint derived in the previous section is expressed as

$$\begin{aligned}\underset{\mathbf{P}, \breve{\mathbf{\Omega}}^k}{\text{minimize}} \quad & \mathrm{tr}\{\mathbf{P}\}\\ \text{subject to} \quad & \zeta_{u,k} \geq \xi_{u,k},\\ & \forall u = 1, 2 \ldots, U, \forall k = 1, 2, \ldots, K,\\ & P_{u,m} \geq 0,\\ & u = 1, 2, \ldots, U, m = 1, 2, \ldots, N_F,\end{aligned} \tag{24}$$

where $\breve{\mathbf{\Omega}}^k$ is the receive filter at the k^{th} MI index.

A. Alternating Optimization

Our objective is to jointly optimize the power allocation at the transmitter and the beamforming vectors at the receiver while the convergence of the iterative receiver is guaranteed. Differentiating the Lagrangian of (24) with respect to the receive beamforming vectors and equating to zero yields

$$\frac{\partial}{\partial \boldsymbol{\omega}^k_{u,m}} \frac{P_{u,m}\boldsymbol{\omega}^{\mathrm{H}}_{u,m}\boldsymbol{\gamma}_{u,m}\boldsymbol{\gamma}^{\mathrm{H}}_{u,m}\boldsymbol{\omega}_{u,m}}{\boldsymbol{\omega}^{\mathrm{H}}_{u,m}\mathbf{\Sigma}_{\hat{\mathbf{r}},m}\boldsymbol{\omega}_{u,m}} = 0. \tag{25}$$

Calculating the derivative in (25) and solving $\boldsymbol{\omega}^k_{u,m}$ results in

$$\begin{aligned}\boldsymbol{\omega}^k_{u,m} =& \frac{\boldsymbol{\omega}^{\mathrm{H}}_{u,m}\mathbf{\Sigma}_{\hat{\mathbf{r}},m}\boldsymbol{\omega}_{u,m}}{P_{u,m}\boldsymbol{\omega}^{\mathrm{H}}_{u,m}\boldsymbol{\gamma}_{u,m}\boldsymbol{\gamma}^{\mathrm{H}}_{u,m}\boldsymbol{\omega}_{u,m}}\boldsymbol{\gamma}^{\mathrm{H}}_{u,m}\boldsymbol{\omega}^k_{u,m}\sqrt{P_{u,m}}\\ & \times (\mathbf{\Sigma}^k_{\hat{\mathbf{r}},m})^{-1}\boldsymbol{\gamma}_{u,m}\sqrt{P_{u,m}},\end{aligned} \tag{26}$$

where $\frac{\boldsymbol{\omega}^{\mathrm{H}}_{u,m}\mathbf{\Sigma}_{\hat{\mathbf{r}},m}\boldsymbol{\omega}_{u,m}}{P_{u,m}\boldsymbol{\omega}^{\mathrm{H}}_{u,m}\boldsymbol{\gamma}_{u,m}\boldsymbol{\gamma}^{\mathrm{H}}_{u,m}\boldsymbol{\omega}_{u,m}} \in \mathbb{R}^+$. Further assuming that $\boldsymbol{\gamma}^{\mathrm{H}}_{u,m}\boldsymbol{\omega}^k_{u,m} \in \mathbb{R}$, the optimal receive beamforming vector for the m^{th} frequency bin of the u^{th} user at the k^{th} MI index is given by

$$\boldsymbol{\omega}^k_{u,m} = \eta^k_u(\mathbf{\Sigma}^k_{\hat{\mathbf{r}},m})^{-1}\boldsymbol{\gamma}_{u,m}\sqrt{P_{u,m}}, \tag{27}$$

where $\mathbf{\Sigma}^k_{\hat{\mathbf{r}},m}$ denotes the interference covariance matrix for the m^{th} frequency bin at the k^{th} MI index and $\eta^k_u \in \mathbb{R}$. The assumption $\boldsymbol{\gamma}^{\mathrm{H}}_{u,m}\boldsymbol{\omega}^k_{u,m} \in \mathbb{R}$ is justified by the fact that the receiver $\boldsymbol{\omega}^k_{u,m}$ can be multiplied by any factor $e^{j\theta}$, $\theta \in [0, 2\pi]$, such that $e^{j\theta}\boldsymbol{\gamma}^{\mathrm{H}}_{u,m}\boldsymbol{\omega}^k_{u,m} \in \mathbb{R}$ without changing the SINR. Hence, the optimal receiver (27) is actually the MMSE receiver used in [24, Chapter 5] up to a scalar multiplier leading to exactly the same SINR. The scaling factor η^k_u should be chosen such that it matches with the assumptions made in the soft demapper. With the notations given in Section III, turbo equalizer works properly only if the scaling factor η^k_u is chosen to be [27] $\eta^k_u = \frac{1}{\mathrm{avg}\{\ddot{\mathbf{b}}^u\}\zeta_{u,k}+1}$.

The joint transmitter-receiver optimization problem can be solved by using the alternating optimization where we split the non-convex joint optimization problem to separate transmitter and receiver optimization. We start with a feasible initial guess[6] $\hat{\mathbf{P}}^{(0)}$ and calculate the optimal receive filter. After that, the problem (24) is solved for a fixed $\breve{\mathbf{\Omega}}^k$. A monotonic convergence of the alternating optimization to a local optima can be justified by the fact that each step improves the objective. The overall algorithm is presented in **Algorithm** 1, where $\mathbf{P}^*$ represents a solution to the problem (24) for fixed $\breve{\mathbf{\Omega}}^k$ and $\breve{\mathbf{\Omega}}^{k*}$ represents the optimal $\breve{\mathbf{\Omega}}^k$ for fixed $\mathbf{P}$. $\Sigma^k_{\hat{\mathbf{r}}} \in \mathbb{C}^{N_R N_F \times N_R N_F}$ is the covariance matrix of the output of the soft cancelation given by

$$\Sigma^k_{\hat{\mathbf{r}}} = \mathbf{\Gamma}\mathbf{P}^{\frac{1}{2}}\mathbf{\Delta}_k\mathbf{P}^{\frac{1}{2}}\mathbf{\Gamma}^{\mathrm{H}} + \sigma^2\mathbf{I}_{N_R N_F}, \tag{28}$$

where $\mathbf{\Delta}_k = \mathbf{I}_{N_U N_F}\bar{\Delta}_k$. In the following sections, we will be focusing on solving the problem (24) for fixed $\breve{\mathbf{\Omega}}^k$, denoted as power allocation problem (PAP).

[5]Equality holds when $I_Z = 0$ or $I_Z = 1$.

[6]Can be found by e.g., using zero forcing algorithm [28].

Algorithm 1 Alternating Optimization.

1) 1: Initialize $\hat{\mathbf{P}} = \hat{\mathbf{P}}^{(0)}$
   2: **repeat**
   3: Calculate the optimal $\breve{\mathbf{\Omega}}^k$ from $\breve{\mathbf{\Omega}}_u^k = \frac{1}{\text{avg}\{\ddot{\mathbf{b}}^u\}\zeta_{u,k}+1}(\mathbf{\Sigma}_{\hat{\mathbf{r}}}^k)^{-1}\mathbf{\Gamma}_u\hat{\mathbf{P}}_u^{\frac{1}{2}}$.
   4: Set $\breve{\mathbf{\Omega}}^k = \breve{\mathbf{\Omega}}^{k*}$ and solve problem (24) with variables $\mathbf{P}$.
   5: Update $\hat{\mathbf{P}} = \mathbf{P}^*$
   6: **until** Convergence

To ease the handling of (24), we write the problem in equivalent form by splitting the convergence constraint into *sum SINR* and *per subcarrier SINR* parts as follows:

$$\frac{1}{N_F}\sum_{m=1}^{N_F} t_{u,m}^k \geq \xi_{u,k}$$

$$t_{u,n}^k = \frac{P_{u,n}|\boldsymbol{\omega}_{u,n}^{k\,\mathrm{H}}\boldsymbol{\gamma}_{u,n}|^2}{\sum_{l=1}^{U} P_{l,n}|\boldsymbol{\omega}_{u,n}^{k\,\mathrm{H}}\boldsymbol{\gamma}_{l,n}|^2\bar{\Delta}_k + \sigma^2||\boldsymbol{\omega}_{u,n}^k||^2}. \quad (29)$$

At the optimal point the constraints hold with equality and hence, we can relax the equality in (29) leading to equivalent formulation

$$\begin{aligned}
\underset{\mathbf{P},\breve{\mathbf{\Omega}}}{\text{minimize}} \quad & \textstyle\sum_{u=1}^{U}\sum_{m=1}^{N_F} P_{u,m} \\
\text{subject to} \quad & \tfrac{1}{N_F}\textstyle\sum_{m=1}^{N_F} t_{u,m}^k \geq \xi_{u,k} \\
& u = 1,2,\ldots,U, k = 1,2,\ldots,K, \\
& \frac{P_{u,n}|\boldsymbol{\omega}_{u,n}^{k\,\mathrm{H}}\boldsymbol{\gamma}_{u,n}|^2}{\sum_{l=1}^{U} P_{l,n}|\boldsymbol{\omega}_{u,n}^{k\,\mathrm{H}}\boldsymbol{\gamma}_{l,n}|^2\bar{\Delta}_k+\sigma^2||\boldsymbol{\omega}_{u,n}^k||^2} \geq t_{u,n}^k, \\
& k = 1,2,\ldots,K, u = 1,2,\ldots,U, \\
& n = 1,2,\ldots,N_F, \\
& P_{u,n} \geq 0, \\
& u = 1,2,\ldots,U, n = 1,2,\ldots,N_F.
\end{aligned} \quad (30)$$

B. Successive Convex Approximation via Variable Change

Similarly to [29], we introduce new variables $\alpha_{u,m} \in \mathbb{R}$, such that $P_{u,m} = e^{\alpha_{u,m}}, \forall u = 1,2,\ldots,U, m = 1,2,\ldots,N_F$. The PAP with new variables can be equivalently written as

$$\begin{aligned}
\underset{\boldsymbol{\alpha},\mathbf{t}}{\text{minimize}} \quad & \textstyle\sum_{u=1}^{U}\sum_{m=1}^{N_F} e^{\alpha_{u,m}} \\
\text{subject to} \quad & \tfrac{1}{N_F}\textstyle\sum_{m=1}^{N_F} t_{u,m}^k \geq \xi_{u,k} \\
& u = 1,2,\ldots,U, k = 1,2,\ldots,K, \\
& \frac{e^{\alpha_{u,n}}|\boldsymbol{\omega}_{u,n}^{k\,\mathrm{H}}\boldsymbol{\gamma}_{u,n}|^2}{\sum_{l=1}^{U} e^{\alpha_{l,n}}|\boldsymbol{\omega}_{u,n}^{k\,\mathrm{H}}\boldsymbol{\gamma}_{l,n}|^2\bar{\Delta}_k+\sigma^2||\boldsymbol{\omega}_{u,n}^k||^2} \geq t_{u,n}^k, \\
& k = 1,2,\ldots,K, u = 1,2,\ldots,U, \\
& n = 1,2,\ldots,N_F,
\end{aligned} \quad (31)$$

where $\mathbf{t} = \{t_{u,m}^k : u = 1,2,\ldots,U, k = 1,2,\ldots,K, m = 1,2,\ldots,N_F\}$, and $\boldsymbol{\alpha} = \{\alpha_{u,m} : u = 1,2,\ldots,U, m = 1,2,\ldots,N_F\}$. Taking the natural logarithm of the *per subcarrier SINR* constraint yields

$$\begin{aligned}
&\alpha_{u,n} + 2\ln(|\boldsymbol{\omega}_{u,n}^{k\,\mathrm{H}}\boldsymbol{\gamma}_{u,n}|) \\
&- \ln(\sum_{l=1}^{U} e^{\alpha_{l,n}}|\boldsymbol{\omega}_{u,n}^{k\,\mathrm{H}}\boldsymbol{\gamma}_{l,n}|^2\bar{\Delta}_k + \sigma^2||\boldsymbol{\omega}_{u,n}^k||^2) \geq \ln t_{u,n}^k.
\end{aligned} \quad (32)$$

It is well known that logarithm of the summation of the exponentials is convex. Hence, the left hand side (LHS) of the constraint (32) is concave. The RHS of (32) can be locally approximated with its best convex upper bound, i.e., linear approximation of $\ln t_{u,n}^k$ at a point $\hat{t}_{u,n}^k$:

$$Y(t_{u,n}^k, \hat{t}_{u,n}^k) = \ln \hat{t}_{u,n}^k + \frac{(t_{u,n}^k - \hat{t}_{u,n}^k)}{\hat{t}_{u,n}^k}. \quad (33)$$

A local convex approximation of (31) can be written as

$$\begin{aligned}
\underset{\boldsymbol{\alpha},\mathbf{t}}{\text{minimize}} \quad & \textstyle\sum_{u=1}^{U}\sum_{m=1}^{N_F} e^{\alpha_{u,m}} \\
\text{subject to} \quad & \textstyle\sum_{m=1}^{N_F} t_{u,m}^k \geq N_F\xi_{u,k}, u = 1,2,\ldots,U, \\
& k = 1,2,\ldots,K, \\
& \alpha_{u,n} + 2\ln(|\boldsymbol{\omega}_{u,n}^{k\,\mathrm{H}}\boldsymbol{\gamma}_{u,n}|) - \\
& \ln(\textstyle\sum_{l=1}^{U} e^{\alpha_{l,n}}|\boldsymbol{\omega}_{u,n}^{k\,\mathrm{H}}\boldsymbol{\gamma}_{l,n}|^2\bar{\Delta}_k + \sigma^2||\boldsymbol{\omega}_{u,n}^k||^2) \geq \\
& Y(t_{u,n}^k, \hat{t}_{u,n}^k), u = 1,2,\ldots,U, \\
& k = 1,2,\ldots,K, n = 1,2,\ldots,N_F,
\end{aligned} \quad (34)$$

and it can be solved efficiently by using standard optimization tools, e.g., interior-point methods [30].

The SCA algorithm starts by a feasible initialization $\hat{t}_{u,n}^k = \hat{t}_{u,n}^{k(0)}, \forall u,k,n$. After this, (34) is solved to obtain a solution $t_{u,n}^{k(*)}$ which is used as a new point for the linear approximation. The procedure is repeated until convergence. The SCA algorithm is summarized in **Algorithm** 2. By projecting the optimal solution from the approximated problem (34) to the original concave function (RHS in (32)) the constraint becomes loose and thus, the objective can always be reduced. Hence, monotonic convergence of the algorithm is guaranteed.

Algorithm 2 Successive convex approximation algorithm.

1: Set $\hat{t}_{u,n}^k = \hat{t}_{u,n}^{k(0)}, \forall u,k,n$.
2: **repeat**
3: Solve Eq. (34).
4: Update $\hat{t}_{u,n}^k = t_{u,n}^{k(*)}, \forall u,k,n$.
5: **until** Convergence.

C. Successive Convex Approximation via Geometric Programming

Another algorithm for solving the PAP can be derived by using the approach introduced in [31] where the SCA is implemented via series of geometric programs (GPs) [30]. The inequality of weighted arithmetic mean and weighted geometric mean states that for any set of $\Phi_m, \alpha_m > 0$, $m = 1,2,\ldots,N_F$,

$$\frac{\sum_{m=1}^{N_F}\Phi_m\alpha_m}{\Phi} \geq \sqrt[\Phi]{\prod_{m=1}^{N_F}\alpha_m^{\Phi_m}}, \quad (35)$$

where $\Phi = \sum_{m=1}^{N_F}\Phi_m$. Choosing $\Phi_m = \frac{\hat{t}_m}{\sum_{n=1}^{N_F}\hat{t}_n}$, $\hat{t}_m > 0$, $m = 1,2,\ldots,N_F$, and denoting $\alpha_m = \frac{t_m}{\Phi_m}$, we have

$$\sum_{m=1}^{N_F} t_m \geq \prod_{m=1}^{N_F}(\frac{t_m}{\Phi_m})^{\Phi_m}, \quad (36)$$

for all $\Phi_m, t_m > 0$, $m = 1, 2, \ldots, N_F$. Therefore, the summation constraint can be replaced by its monomial underestimate, with which a local approximation of (24) for fixed $\breve{\mathbf{\Omega}}^k$ can be derived in the form of GP, as

$$\begin{aligned}
\underset{\mathbf{P},\mathbf{t}}{\text{minimize}} \quad & \text{tr}\{\mathbf{P}\} \\
\text{subject to} \quad & \textstyle\prod_{n=1}^{N_F} \left(\frac{t_{u,n}^k}{\Phi_{u,n}^k}\right)^{\Phi_{u,n}^k} \geq N_F \xi_{u,k}, \\
& u = 1, 2, \ldots, U, k = 1, 2, \ldots, K, \\
& P_{u,m} |{\boldsymbol{\omega}_{u,m}^k}^{\mathrm{H}} \boldsymbol{\gamma}_{u,m}|^2 \geq \\
& \left(\textstyle\sum_{l=1}^{U} P_{l,m} |{\boldsymbol{\omega}_{u,m}^k}^{\mathrm{H}} \boldsymbol{\gamma}_{l,m}|^2 \bar{\Delta}_k + \sigma^2 |\boldsymbol{\omega}_{u,m}^k|^2\right) t_{u,m}^k, \\
& u = 1, 2, \ldots, U, k = 1, 2, \ldots, K, \\
& m = 1, 2, \ldots, N_F, \\
& P_{u,m} \geq 0, \quad u = 1, 2, \ldots, U, m = 1, 2, \ldots, N_F.
\end{aligned} \tag{37}$$

Now the objective is a posynomial, the LHSs of the inequality constraints are monomials and the RHSs are posynomials. Hence, (37) is in the form of GP, which can be transformed to a convex optimization problem [30]. Now, **Algorithm** 2 can be used by replacing (34) in step 3 by (37). Because the monomial approximation is never above the approximated summation (36), the same arguments describing the convergence presented in Sec. V-B apply also in this case. Hence, it is guaranteed that SCA with approximation (37) converges monotonically.

The motivation of introducing two different SCAs, via variable change and via GP is to give alternative approaches for the implementation of the optimization algorithm. The main difference is in the approximated constraints: In (34), per subcarrier constraint is approximated and the number of the approximated constraints is UN_FK. In (37), sum SINR constraint is approximated and the number of approximated constraints is UK.

VI. Numerical Results

In this section, we show the results obtained by simulations to evaluate the performance of the proposed algorithms. The following abbreviations for the algorithms are used: SCAVC stands for the successive convex approximation via variable change presented in Section V-B and SCAGP denotes the successive convex approximation via geometric programming presented in Section V-C. The stopping criterion of **Algorithm** 1 and **Algorithm** 2 is that the change in the objective function becomes less than or equal to a small specific value between two consecutive iterations. In simulations, we set the stopping threshold value at 0.05 for **Algorithm** 1 and 0.01 for **Algorithm** 2. EP denotes the single carrier transmission without precoding, i.e., equal power is allocated for all users across the frequency band, where the power level satisfying the convergence constraints is found by using the bisection algorithm [30].

We also simulated the system with the best possible orthogonal allocation obtained by performing exhaustive search (OES) over all possible subcarrier combinations. Orthogonal in this context indicates that only one user is active in each subcarrier at a time. The convergence constraint for OES can be written as

$$\frac{1}{N_F} \sum_{m \in \mathcal{N}_F^u} \frac{P_{u,m} ||\boldsymbol{\gamma}_{u,m}||^2}{P_{u,m} ||\boldsymbol{\gamma}_{u,m}||^2 \bar{\Delta}_k + \sigma^2} \geq \xi_{u,k}, \tag{38}$$

where $\mathcal{N}_F^u$ is the set of frequency bins allocated to user u and $\mathcal{N}_F^l \cap \mathcal{N}_F^u = \varnothing$, $\forall l \neq u$, $\bigcup_{u=1}^{U} \mathcal{N}_F^u = \mathcal{N}_F$. Clearly, (38) is a convex constraint $\forall k, u$.

We also considered a receiver structure where spatial zero forcing (ZF) [28] is concatenated with FD-SC-MMSE (ZF-SCMMSE). The constraint for ZFSCMMSE is then written as

$$\frac{1}{N_F} \sum_{m=1}^{N_F} \frac{P_{u,m}}{P_{u,m} \bar{\Delta}_k + \sigma^2 ||\mathbf{w}_{u,m}||^2} \geq \xi_{u,k}, \tag{39}$$

where $\mathbf{w}_{u,m}$ is the ZF beamforming vector for the u^{th} user at the m^{th} frequency bin. Clearly, (39) is a convex constraint $\forall k, u$. It can be seen from (38) and (39) that there is no inter-user-interference in OES and ZFSCMMSE. Therefore, OES and ZFSCMMSE are simplified to a single user loading [13].

The results were obtained with the following parameters: $N_F = 8$, QPSK ($N_Q = 2$) and 16QAM ($N_Q = 4$) with Gray mapping, and systematic repeat accumulate (RA) code [32] with a code rate 1/3 and 8 internal iterations. The number of EXIT samples is either $K = 1$ or $K = 5$. In case of $K = 1$ only one of the convergence constraints for each user is taken into account. More specifically, it means that $\hat{I}_u^{\text{A,target}} = 0$, and $\hat{I}_{u,k}^{\text{E}} = \hat{I}_u^{\text{E,target}}$, $u = 1, 2$, $k = K$. The feedback from the decoder is not taken into account and hence, it corresponds to the linear equalizer. In case of $K = 5$ the points were placed uniformly along the line from the origin to the convergence point, i.e., uniformly over $[0, \hat{I}^{\text{E,target}}]$. The signal-to-noise ratio per receiver antenna averaged over frequency bins is defined by SNR$= \text{tr}\{\mathbf{P}\}/(N_R N_F \sigma^2)$. We considered two different channel conditions, namely, a static 5-path channel where path gains were generated randomly, and a quasi-static Rayleigh fading 5-path average equal gain channel.

For verifying the accuracy of the method, EXIT simulations were carried out in a static channel, and the trajectories were obtained through chain simulations with a random interleaver of size 240000 bits. The EXIT curve of the decoder was obtained by using 200 blocks for each a priori value with the size of a block being 6000 bits. The EXIT curves of the equalizer with SCAGP and the decoder as well as the trajectories for two and four users with QPSK and 16QAM are depicted in Fig. 5. It is found that when $U = 2$ and QPSK is used, the gap between the EXIT curves satisfies the preset condition and the convergence points are very close to the preset values. Furthermore, the trajectory matches closely to the EXIT curves which indicates that the algorithm works properly. When the modulation order is increased to 16QAM there exists a slight discrepancy between the EXIT curves and the trajectory. This is because of the inequality shown in (23). Due to the conservativeness of the convergence constraint in the case of 16QAM, the real chain simulation provides larger MI than the approximated EXIT curves and hence, the actual trajectory reaches the convergence point. Therefore, since the constraint in (24) provides an upper bound, the convergence is guaranteed also with 16QAM.

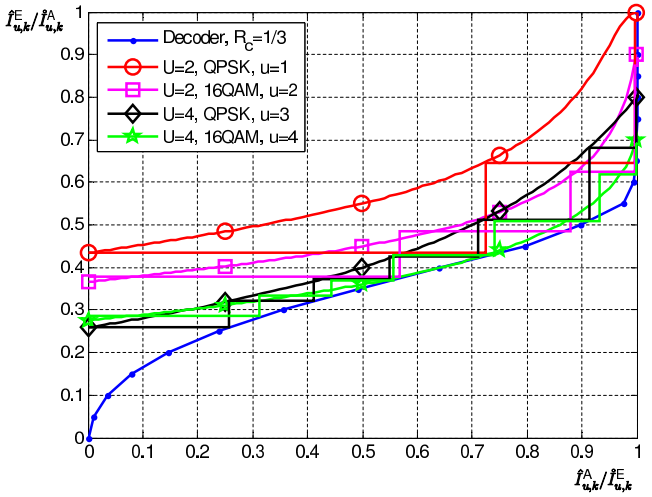

Fig. 5. Verification EXIT chart in static channel for SCAGP with $N_F = 8$, $K = 5$, $N_R = U$, $\mathring{I}_u^{\mathrm{E,target}} = 0.9999$, $\forall u$, $(\hat{I}_1^{\mathrm{E,target}}, \hat{I}_2^{\mathrm{E,target}}, \hat{I}_3^{\mathrm{E,target}}, \hat{I}_4^{\mathrm{E,target}}) = (0.9999, 0.9, 0.8, 0.7)$ and $(\epsilon_1, \epsilon_2, \epsilon_3, \epsilon_4) = (0.2, 0.1, 0.05, 0.01)$. When $U = 2$, parameters of users 1 and 2 are used.

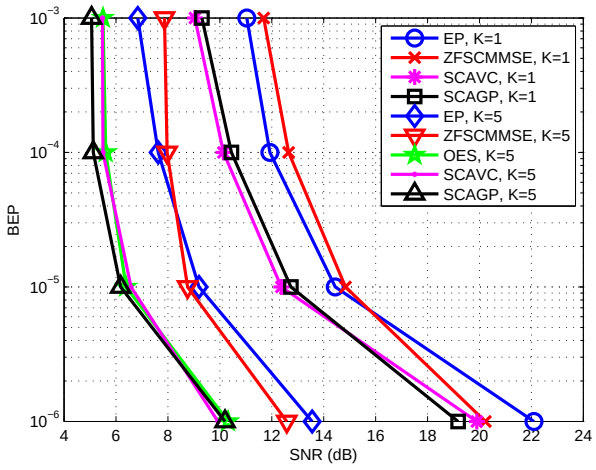

Fig. 6. The *a posteriori* BEP comparison. $U = 2$, $N_F = 8$, $N_R = 2$, targets = $[10^{-3}, 10^{-4}, 10^{-5}, 10^{-6}]$, $\epsilon_u = 0.1$, $\forall u$.

To obtain further insight of the tradeoff between ϵ_u and the required SNR to satisfy the constraints we tested all the algorithms shown in this paper in a static channel with various ϵ_u, and evaluated the SNR value and the number of iterations required to achieve the target point. The results are shown in Table I. It can be seen that decreasing ϵ_u from 0.2 to 0.1 requires only one or two more iterations and the required SNR can be decreased roughly 1 dB, depending on the algorithm used. The required SNR can be further reduced by about 0.5 dB by decreasing ϵ_u to 0.01 while the number of iterations increased approximately three times.

For QPSK, MI target can be converted to bit error probability (BEP) by using the equation [8]

$$P_b \approx \frac{1}{2}\mathrm{erfc}\left(\frac{\sqrt{\mathrm{J}_2^{-1}(\hat{I}_1^{\mathrm{A,target}}) + \mathrm{J}_2^{-1}(\hat{I}_1^{\mathrm{E,target}})}}{2\sqrt{2}}\right). \quad (40)$$

In Fig. 6, required SNR versus BEP is presented, where four different BEP target values are considered for $u = 1, 2$, namely 10^{-3}, 10^{-4}, 10^{-5}, 10^{-6} corresponding to the MI targets $(\mathring{I}_u^{\mathrm{E,target}}, \hat{I}_u^{\mathrm{E,target}}) = (0.99, 0.6185)$, $(\mathring{I}_u^{\mathrm{E,target}}, \hat{I}_u^{\mathrm{E,target}}) = (0.9987, 0.673)$, $(\mathring{I}_u^{\mathrm{E,target}}, \hat{I}_u^{\mathrm{E,target}}) = (0.9998, 0.7892)$, $(\mathring{I}_u^{\mathrm{E,target}}, \hat{I}_u^{\mathrm{E,target}}) = (0.9998, 0.9819)$, respectively. It can be seen that OES, SCAGP and SCAVC achieve the best result when $K = 5$. ZFSCMMSE and EP with $K = 5$ are 1.3 dB - 3.6 dB worse in terms of SNR, depending on the BEP target and the algorithm used.

It is worth noticing that the solution obtained by SCAGP and SCAVC in this particular case is very close to the orthogonal solution (OES). This is due to the fact that when $\bar{\Delta}^l = 0$, $\forall l = 1, 2, \ldots, U$ in (11) all the interference is canceled and the optimal receiver is the filter matched to the channel. In this case, the optimal allocation strategy to maximize (10) is to allocate power on the strongest bin. However, this would not necessarily satisfy the constraint in (24) if $\bar{\Delta}_k = 1$. Thus, the power has to be distributed to several bins which results in higher power consumption. Hence, if the tightest constraint, i.e., $\bar{\Delta}_k = 1$, can be satisfied by using only one frequency bin, it is indeed the best solution. This is the case when the interference level is low, as shown in the case presented in Fig. 6. When the number of users increases, interference also increases and the orthogonal solution may not be feasible. This can be seen by rewriting (38) into the form of

$$\sum_{m \in \mathcal{N}_F^u} \frac{1}{P_{u,m}||\boldsymbol{\gamma}_{u,m}||^2 \bar{\Delta}_k + \sigma^2} \leq \frac{N_F^u - \xi_{u,k} N_F \bar{\Delta}_k}{\sigma^2}, \quad (41)$$

where N_F^u is the cardinality of the set $\mathcal{N}_F^u$. From the non-negativity of the right hand side (RHS) of Eq. (41) we get a necessary constraint for the minimum number of the frequency bins that has to be allocated to user u as

$$N_F^u \geq \xi_{u,k} N_F \bar{\Delta}_k, \quad \forall k = 1, 2, \ldots, K. \quad (42)$$

As it was seen in Section IV, $\xi_{u,k}$ and $\bar{\Delta}_k$ depend on the channel code used. Thus, we can conclude that the feasibility of OES algorithm can be controlled by varying the channel code. The following results are presented for 16QAM only with $R_c = 1/3$ where the OES algorithm is not feasible due to (42).

Fig. 7 shows the minimum SNR required to achieve the corresponding MI target for user 1 for each of the proposed algorithms for $U = 2$. It is found that the SNR gain by precoding with $K = 5$ is significant compared to precoding with $K = 1$. The SNRs with SCAGP and SCAVC are approximately equal and they provide the best results in terms of SNR. As expected, EP with $K = 1$ requires the highest SNR among all the algorithms tested.

Fig. 8 shows the minimum SNR required to achieve the corresponding MI target for user 1 for each of the proposed algorithms for $U = 4$. The results are similar to the case of $U = 2$: ZFSCMMSE with $K = 5$ requires more power than EP with $K = 5$ when the MI target is low. However, when MI target increases ZFSCMMSE performs better than EP with $K = 5$.

TABLE I

REQUIRED SNR AND NUMBER OF ITERATIONS WITH VARIOUS ϵ. THE ELEMENTS IN THE TABLE ARE IN THE FORM OF SNR(DB) / ITERATIONS FOR USER 1 / ITERATIONS FOR USER 2. $U = 2$, $N_R = 2$, $N_Q = 2$, $K = 5$, $\hat{I}_u^{\text{A,TARGET}} = 0.9999$, $\forall u$, $\hat{I}_1^{\text{E,TARGET}} = 0.7$, $\hat{I}_1^{\text{E,TARGET}} = 0.9$.

$\epsilon_1 = \epsilon_2$	OES	SCAGP	SCAVC	ZFSCMMSE	EP
0.01	4.56 / 19 / 18	4.53 / 20 / 18	4.53 / 18 / 17	6.56 / 10 / 10	8.82 / 3 / 3
0.1	5.29 / 6 / 6	5.10 / 6 / 5	5.11 / 6 / 5	7.08 / 5 / 5	8.82 / 3 / 3
0.2	6.89 / 4 / 4	6.12 / 4 / 4	6.13 / 4 / 3	7.96 / 3 / 3	8.82 / 3 / 3

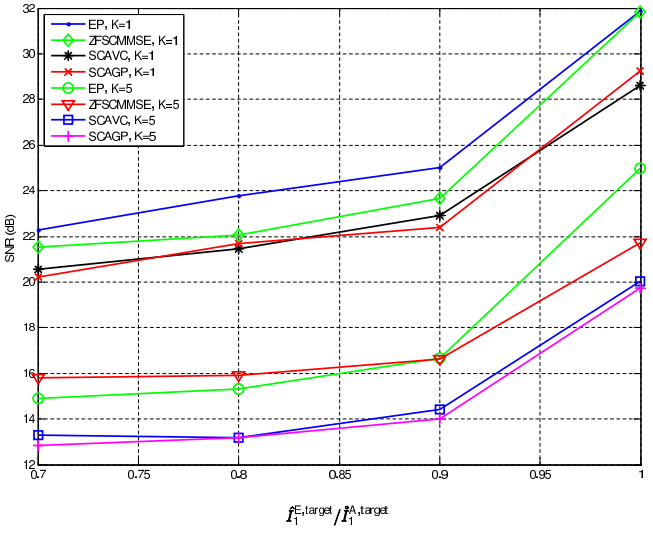

Fig. 7. SNR using the corresponding MI target for user 1. $U = 2$, $N_F = 8$, $N_R = 2$, $N_Q = 4$, $\hat{I}_2^{\text{E,target}} = 0.8$, $\hat{I}_u^{\text{E,target}} = 0.9999$, $u = 1, 2$, $\epsilon_u = 0.1$, $u = 1, 2$, $N_L = 5$.

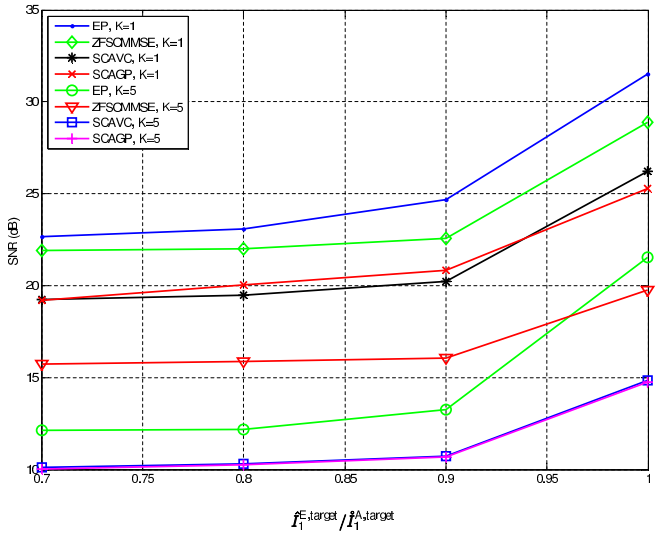

Fig. 8. SNR using the corresponding MI target for user 1. $U = 4$, $N_F = 8$, $N_R = 4$, $N_Q = 4$, $\hat{I}_u^{\text{E,target}} = 0.8$, $u = 2, 3, 4$, $\hat{I}_u^{\text{E,target}} = 0.9999$, $\forall u$, $\epsilon_u = 0.1$, $\forall u$, $N_L = 5$.

As seen in Section V, both SCAGP and SCAVC are to be solved via a series of convex problems. For solving convex problems, many efficient tools are known in the literature [30]. Hence, the complexity analysis boils down to the comparison of how many times the optimization problem needs to be solved for each of the algorithms to achieve the convergence according to the criteria described at the beginning of this section. The number of the solver call times that **Algorithm** 1 needs varies typically between 1 - 9 depending on the simulation setup. The more users, the more iterations is needed. The number of the solver call times that **Algorithm** 2 needs in **Algorithm** 1 varies between 1 - 13.

The motivation of using single carrier FDMA is its favorable PAPR properties. The PAPR of EP is only 2.55 dB for 16QAM due to the equal sizes of DFT and IDFT at the transmitter and receiver. However, the PAPR is increased when power allocation is performed across the frequency band. To demonstrate the trade off between a reduction of the required SNR and an increase in PAPR, we measured the PAPR at the output of IFFT in the transmitter and evaluated the complementary cumulative distribution functions (CCDF) Prob$(PAPR > \delta)$ for algorithms investigated in this paper. The results are shown in Fig. 9, where δ corresponds to the PAPR value on the horizontal axis. It can be seen that unequal power allocation increases the PAPR significantly. Furthermore, with $K = 5$ the PAPR is higher than with $K = 1$ because with $K = 5$, the power allocation tends to be more orthogonal. However, it can be seen from Fig. 8 that the required SNR is reduced.

The maximum transmission power is defined as $P_{\max}(dB) = P_{\text{avg}}^u(dB) + PAPR(dB)$, where $P_{\text{avg}}^u = \frac{SNR \times N_R \times \sigma^2}{U}$ denotes the average power of user u. Let us consider an example where the maximum transmission power is to be configured according to 8 dB PAPR which corresponds to $10^{-2.92}$ value in CCDF for SCAGP and $K = 5$. For that same value of CCDF, the PAPR is 5.14 dB for SCAGP and $K = 1$. Hence, increasing K from one to five the total power gain is $P_{\max}(dB)^{\text{SCAGP,K=1}} - P_{\max}(dB)^{\text{SCAGP,K=5}} = 15.28dB + 5.14dB - 4.76dB - 8dB = 7.66dB$. Therefore, the increase of K from 1 to 5 significantly increases the coverage of the precoded transmission. However, SCAGP with $K = 5$ requires 6.8 dB lower SNR than EP with $K = 5$. Using the same 8 dB example as above, the total power gain is 6.7 dB - (8 dB - 2.55 dB) = 1.25 dB. However, this is only the worst case comparison, i.e., DFT and IDFT sizes are not necessarily equal in practice, and the use of different sizes of DFT and IDFT results in the increase of PAPR of EP algorithm [33]. As a conclusion, even with the worst case comparison, SCAVC and SCAGP can achieve a significantly larger coverage than EP with a significantly lower average

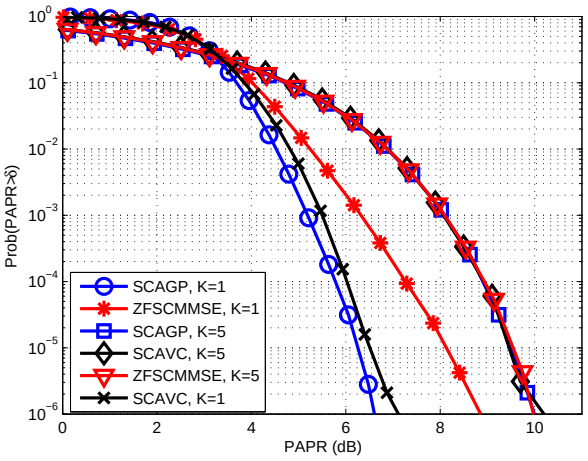

Fig. 9. CCDF for user 1. $U = 4$, $N_F = 8$, $N_R = 4$, $N_Q = 4$, $\hat{I}_1^{\text{E,target}} = 0.9999$, $\hat{I}_u^{\text{E,target}} = 0.8$, $u = 2, 3, 4$, $\hat{I}_u^{\text{E,target}} = 0.9999$, $\forall u$, $\epsilon_u = 0.1$, $\forall u$, $N_L = 5$.

power consumption.

VII. Conclusions

In this paper, we have derived a convergence constrained power allocation (CCPA) problem for the iterative frequency domain multiuser SIMO detector. Furthermore, with our novel problem derivation the generalization for higher order modulations is straightforward. Moreover, we derived two successive convex approximations for finding a local solution to the problem. Numerical results indicate that significant gains in terms of average power consumption can be achieved compared to the linear receivers with and without precoding as well as to the iterative receiver without precoding. Furthermore, it was shown that the peak-to-average power ratio (PAPR) increase due to precoding is relatively small compared to the gain in the average power consumption. Thus, the maximum cell size is increased by the use of precoding. The algorithms proposed in this work allow the utilization of the iterative receiver and its convergence properties also at the transmitter side.

References

[1] D. Falconer, S. L. Ariyavisitakul, A. Benyamin-Seeyar, and B. Eldson, "Frequency domain equalization for single-carrier broadband wireless systems," *IEEE Commun. Mag.*

[2] R. W. Chang, "Synthesis of band-limited orthogonal signals for multichannel data transmission," *Bell System Technical Journal*.

[3] F. Pancaldi, G. Vitetta, R. Kalbasi, N. Al-Dhahir, M. Uysal, and H. Mheidat, "Single-carrier frequency domain equalization," *Signal Processing Magazine, IEEE*, vol. 25, no. 5, pp. 37–56, 2008.

[4] R. V. Nee and R. Prasad, *OFDM for Wireless Multimedia Communications*. Norwood, MA: Artech House, 2000.

[5] K. Kansanen, T. Matsumoto, C. Schneider, and R. Thoma, "Frequency-domain MMSE turbo equalization of multilevel coded QAM-convergence in real fields," in *Personal, Indoor and Mobile Radio Communications, 2005. PIMRC 2005. IEEE 16th International Symposium on*, vol. 2, 2005, pp. 1019–1023 Vol. 2.

[6] X. Yuan, Q. Guo, X. Wang, and L. Ping, "Evolution analysis of low-cost iterative equalization in coded linear systems with cyclic prefix," *IEEE J. Select. Areas Commun.*, vol. 26, no. 2, pp. 301–310, Feb. 2008.

[7] D. Shepherd, Z. Shi, M. Reed, and F. Schreckenbach, "Optimization of unequal power coded multiuser DS-CDMA using extrinsic information transfer charts," in *Proc. Conf. Inform. Sciences Syst. (CISS)*, Princeton, USA, Mar. 2006.

[8] S. ten Brink, "Convergence behavior of iteratively decoded parallel concatenated codes," *IEEE Trans. Commun.*, vol. 49, no. 10, pp. 1727–1737, Oct. 2001.

[9] X. Yuan, H. Li, L. Ping, and X. Lin, "Precoder design for ISI channels based on iterative LMMMSE equalization," in *Proc. Int. Symp. on Turbo Codes and Related Topics*, Lausanne, Switzerland, Sep.1–5 2008, pp. 198–203.

[10] J. Karjalainen and T. Matsumoto, "On the convergence property of an MMSE multiuser MIMO turbo detector with uplink precoding," in *Proc. IEEE Int. Conf. Commun.*, Beijing, China, May19–23 2008.

[11] J. Karjalainen, T. Matsumoto, and W. Utschick, "Convergence analysis of MMSE based multiuser MIMO turbo detector with linear precoding strategies," in *Proc. Int. Symp. on Turbo Codes and Related Topics*, Lausanne, Switzerland, Sep.1–5 2008.

[12] X. Yuan, C. Xu, L. Ping, and X. Lin, "Precoder Design for Multiuser MIMO ISI Channels Based on Iterative LMMSE detection," *Selected Topics in Signal Processing, IEEE Journal of*, vol. 3, no. 6, pp. 1118–1128, 2009.

[13] J. Karjalainen, M. Codreanu, A. Tölli, M. Juntti, and T. Matsumoto, "EXIT chart-based power allocation for iterative frequency domain MIMO detector," *IEEE Trans. Signal Processing*, vol. 59, no. 4, pp. 1624–1641, Apr. 2011.

[14] S. ten Brink, "Convergence behavior of iterative decoding," *IEE Electron. Lett.*

[15] A. Ashikhmin, G. Kramer, and S. ten Brink, "Extrinsic information transfer functions: Model and erasure channel properties," *IEEE Trans. Inform. Theory*.

[16] F. Brännström, L. K. Rasmussen, and A. J. Grant, "Convergence analysis and optimal scheduling for multiple concatenated codes," *IEEE Trans. Inform. Theory*, vol. 51, no. 9, pp. 3354–3364, Sep. 2005.

[17] S. ten Brink, G. Kramer, and A. Ashikhmin, "Design of low-density parity-check codes for modulation and detection," *Communications, IEEE Transactions on*, vol. 52, no. 4, pp. 670–678, 2004.

[18] S. ten Brink and G. Kramer, "Design of repeat-accumulate codes for iterative detection and decoding," *Signal Processing, IEEE Transactions on*, vol. 51, no. 11, pp. 2764–2772, 2003.

[19] 3rd Generation Partnership Project (3GPP); Technical Specification Group Radio Access Network Evolved Universal Terrestrial Radio Access E-UTRA, "Physical channels and modulation 3GPP TS 36.211 Version 12.1.0 (Release 12)," Tech. Rep., 2014.

[20] D. P. Bertsekas, *Nonlinear Programming*. Cambridge, U.K.: Cambridge Univ. Press, 2005.

[21] A. Wiesel, Y. Eldar, and S. Shamai, "Linear precoding via conic optimization for fixed mimo receivers," *Signal Processing, IEEE Transactions on*, vol. 54, no. 1, pp. 161–176, Jan 2006.

[22] B. Marks and G. Wright, "A general inner approximation algorithm for nonconvex mathematical programs," *Journal of the Operations Research Society of America*, vol. 26, no. 4, pp. 681–683, 1987.

[23] M. Tüchler, A. C. Singer, and R. Koetter, "Minimum mean squared error equalization using *a priori* information," *IEEE Trans. Signal Processing*, vol. 50, no. 3, pp. 673–683, Mar. 2002.

[24] J. Karjalainen, "Broadband single carrier multi-antenna communications with frequency domain turbo equalization," Ph.D. dissertation, University of Oulu, Oulu, Finland, 2011. [Online]. Available: http://herkules.oulu.fi/isbn9789514295027/isbn9789514295027.pdf

[25] F. Brännström, "Convergence analysis and design of multiple concatenated codes," Ph.D. dissertation, Chalmers University of Technology, Gothenburg, Sweden, 2004.

[26] V. Ramon, C. Herzet, and L. Vandendorpe, "A semi-analytical method for predicting the performance and convergence behavior of a multiuser turbo-equalizer/demapper," *Signal Processing, IEEE Transactions on*, vol. 55, no. 3, pp. 1104–1117, 2007.

[27] K. Kansanen and T. Matsumoto, "An analytical method for MMSE MIMO turbo equalizer EXIT chart computation," *Wireless Communications, IEEE Transactions on*, vol. 6, no. 1, pp. 59–63, 2007.

[28] D. Tse and P. Viswanath, *Fundamentals of Wireless Communication*. Cambridge, U.K.: Cambridge Univ. Press, 2005.

[29] J. Kaleva, A. Tölli, and M. Juntti, "Weighted Sum Rate Maximization for Interfering Broadcast Channel via Successive Convex Approximation," in *Proc. IEEE Global Telecommun. Conf.*, Dec. 2012.

[30] S. Boyd and L. Vandenberghe, *Convex Optimization*. Cambridge, U.K.: Cambridge Univ. Press, 2004.

[31] M. Chiang, C. wei Tan, D. Palomar, D. O'Neill, and D. Julian, "Power control by geometric programming," *Wireless Communications, IEEE Transactions on*, vol. 6, no. 7, pp. 2640–2651, 2007.

[32] D. Divsalar, H. Jin, and R. J. McEliece, "Coding theorems for 'turbo-like' codes," in *Proc. Annual Allerton Conf. Commun., Contr., Computing*, Urbana, Illinois, USA, Sep.23–25 1998, pp. 201–210.
[33] C. Yuen and B. Farhang-Boroujeny, "Analysis of the optimum precoder in SC-FDMA," *Wireless Communications, IEEE Transactions on*, vol. 11, no. 11, pp. 4096–4107, 2012.

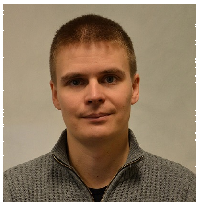

Valtteri Tervo (S'10) received his M.Sc degree in Telecommunications from the University of Oulu, Oulu, Finland in September 2009. Currently he is pursuing his doctoral degree under the dual degree program between the University of Oulu and Japan Advanced Institute of Science and Technology (JAIST). From the beginning of 2015, V. Tervo has been working as a work package leader in an FP7 project Links-on-the-fly Technology for Robust, Efficient and Smart Communication in Unpredictable Environments (RESCUE). His main research interests are in power allocation and transceiver design for broadband wireless communications with special emphasis on iterative reception.

Antti Tölli (M'08, SM'14) received his Dr.Sc (Tech) degree in electrical engineering from the University of Oulu, Oulu, Finland in June 2008. Before joining the Department of Communication Engineering (DCE) and Centre for Wireless Communications (CWC) at the University of Oulu, he worked five years for Nokia Networks, IP Mobility Networks division as a Research Engineer and Project Manager both in Finland and Spain. Currently he works as an Adjunct Professor and Academy Research Fellow at the DCE of the University of Oulu. His main research interests are in radio resource management and transceiver design for broadband wireless communications with special emphasis on interference management in multiuser MIMO cellular systems. A. Tölli has published more than 100 papers and several patents all in the area of signal processing and wireless communications.

Juha Karjalainen (S'03-M'10) received his M.Sc.(Tech.) and Dr.Sc degree in electrical engineering from University of Oulu, Finland, in 2001 and 2011. Currently, he is working at Nokia Networks, Finland, as a Senior Specialist. Before he joined to Nokia Networks, he was working with Samsung Electronics as a Principal Standards Engineer. Prior to that, he was working at Renesas Mobile as a Principal Researcher, and with University of Oulu as a Research Scientist and Project Manager as well as Nokia Mobile Phones working as Senior Designer. His research interests include next generation mobile broadband communication systems, multi-antenna transceiver schemes and interference management.

Tad Matsumoto (S'84-SM'95-F'10) received the B.S., M.S., and Ph.D. degrees from Keio University, Yokohama, Japan, in 1978, 1980, and 1991, respectively, all in electrical engineering. He joined Nippon Telegraph and Telephone Corporation (NTT) in April 1980. Since he engaged in NTT, he was involved in a lot of research and development projects, all for mobile wireless communications systems. In July 1992, he transferred to NTT DoCoMo, where he researched Code-Division Multiple-Access techniques for Mobile Communication Systems. In April 1994, he transferred to NTT America, where he served as a Senior Technical Advisor of a joint project between NTT and NEXTEL Communications. In March 1996, he returned to NTT DoCoMo, where he served as a Head of the Radio Signal Processing Laboratory until August of 2001. He worked on adaptive signal processing, multiple-input multiple-output turbo signal detection, interference cancellation, and space-time coding techniques for broadband mobile communications. In March 2002, he moved to University of Oulu, Finland, where he served as a Professor at the Centre for Wireless Communications. In 2006, he served as a Visiting Professor at Ilmenau University of Technology, Ilmenau, Germany, funded by the German MERCATOR Visiting Professorship Program. Since April 2007, he has been serving as a Professor at the Japan Advanced Institute of Science and Technology (JAIST), Japan, while also keeping the position at University of Oulu. He was appointed a Finland Distinguished Professor for a period from January 2008 to December 2012, funded by the Finnish National Technology Agency (Tekes) and Finnish Academy, under which he preserves the rights to participate in and apply to European and Finnish national projects. He is a recipient of the IEEE VTS Outstanding Service Award (2001), Nokia Foundation Visiting Fellow Scholarship Award (2002), IEEE Japan Council Award for Distinguished Service to the Society (2006), IEEE Vehicular Technology Society James R. Evans Avant Garde Award (2006), and Thuringen State Research Award for Advanced Applied Science (2006), 2007 Best Paper Award of Institute of Electrical, Communication, and Information Engineers of Japan (2008), Telecom System Technology Award by the Telecommunications Advancement Foundation (2009), IEEE Communication Letters Exemplifying Reviewer Award (2011), and Nikkei Wireless Japan Award (2012). He is a member of IEICE. He is serving as an IEEE Vehicular Technology Distinguished Lecturer during the term July 2011-June 2015.